Cost-Efficient Design of an Energy-Neutral UAV-Based Mobile Network

M. Virgili, *Student Member, IEEE,* N. Babu, *Student Member, IEEE,* M. Javidsharifi, *Student Member, IEEE,* I. Valiulahi, *Student Member, IEEE,* C. Masouros, *Senior Member, IEEE,* A. J. Forsyth, *Senior Member, IEEE,* T. Kerekes, *Senior Member, IEEE,* C. B. Papadias, *Fellow, IEEE.*

***Abstract*—This work proposes a framework to design a cost-efficient unmanned aerial vehicle (UAV)-based energy-neutral (EN) system deployed to harvest data from a set of internet-of-things (IoT) nodes. The energy-neutrality refers to the zero-sum balance between energy harvested, stored, and consumed during operation, which is a game-changer when a connection to the electricity grid is not available/feasible. This involves employing an off-grid charging station (CS) comprising of photovoltaic (PV) panels and batteries that provide enough energy to recharge the UAV-based aerial access points (AAPs). The investment cost is determined by the number of AAPs, PV panels, and ground battery units. Its minimization cannot be achieved using conventional optimization tools due to the non-tractable form of the CS load. Therefore, a novel wave-based method is proposed to represent the load profile as a proportional function of the required number of AAPs, so as to directly relate the CS design to the trajectory optimization. Compared to baseline scenarios, the proposed trajectory design can halve the time and energy consumption; the investment cost varies with the time and season of service; the off-grid CS is particularly advantageous in rural areas, while in urban areas its cost is comparable to that of a grid-connected alternative.**

***Index Terms*—Communication systems, solar energy, energy storage, load modeling, remotely piloted aircraft.**

I. Introduction

THE use of unmanned aerial vehicle(s) (UAVs) provisioned with on-board next-generation small cell radio access node as aerial access point(s) (AAPs) to harvest data from a set of Internet-of-Things (IoT) nodes has gained much attention in the recent years [1]. A separate study item has been released by the third generation partnership project (3GPP) detailing the architecture and link-level requirements of an AAP [2]. If the system is deployed for a short-term event, such as data harvesting from a rural IoT network that is widely spread geographically, deploying a grid-connected fixed infrastructure would be cost-inefficient, since this would require a large number of telco modules with under-utilized capacity. Additionally, a connection node to the electricity grid may not be available in some areas, and installing one might not be feasible due to the high installation costs. A potential solution to this is to employ an off-grid system that harvests (and stores) the required energy from the surrounding environment. In the proposed instance, the system is a UAV-based mobile network that consists of a set of UAVs and a ground charging station (CS). By virtue of limited on-board battery capacity, the available service time of an active (flying) AAP is a function of the on-board battery pack and its trajectory; consequently, in order to guarantee continuity of service beyond the active time of a single AAP, a set of fully charged idle (not active) AAPs is needed, so as to replace the out-of-power AAP(s), as shown in Fig. 1. Moreover, given the high cost of AAPs, the out-of-power AAP should be recharged while its replacement is active, thereby justifying the use of a CS. Hence, to guarantee 100% reliability, the load to the CS should be modeled as a function of the UAV-and mission-related time factors, such as the active time of a UAV, time between successive data harvesting from an IoT node, etc. Inspired by the above facts, in this work, we model both the energy demand and supply of an energy-neutral (EN) UAV-based mobile network as respective functions of the mission-related time factors and the solar irradiation. These are then used to develop a general framework that uses the trajectory of the AAP as a tool to minimize the investment cost.

A. Related Works

The sizing of a photovoltaic (PV)-battery system for supplying a CS is challenging due to factors such as the associated costs, the volatility of solar irradiation, varying load, and physical location constraints [3]. The focus of the work in [3] - [8] is on supplying the energy required by base stations in mobile networks through PV-battery systems. In [3] and [4], the authors optimize the size of the energy system used to power a fixed telecommunication infrastructure, but they do not control the load profile, which is taken as a design requirement. The works in [5] and [6] model the performance of renewable energy source (RES)-based base stations to size the energy system based on Markovian models. [7] proposes a multi-objective wind-driven optimization (MO-WDO) algorithm to size an off-grid energy system. The number of PV panels and battery cells are optimized based on the 'annual total life cycle cost'. In [8], a genetic algorithm-based methodology is

M. Virgili is with Lyra Electronics (e-mail: mvirgili@lyraelectronics.com).
M. Virgili and A. J. Forsyth are with The University of Manchester (e-mail: marco.virgili@postgrad.manchester.ac.uk, andrew.forsyth@manchester.ac.uk).
N. Babu and C. B. Papadias are with Research, Technology and Innovation Network (RTIN), Alba, The American College of Greece, Greece (e-mail: {nbabu, cpapadias}@acg.edu).
N. Babu and C. B. Papadias are with Department of Electronic Systems, Aalborg University, Denmark (e-mail: {niba, copa}@es.aau.dk).
M. Javidsharifi and T. Kerekes are with Department of Energy, Aalborg University (e-mail: {mja, tak}@energy.aau.dk).
I. Valiulahi and C. Masouros are with University College of London (e-mail: {i.valiulahi, c.masouros}@ucl.ac.uk).

proposed to design a PV-battery system with the objectives of minimizing CAPEX and OPEX. The load profile to the charging station used in [3]- [8] is not suitable for a UAV-based mobile network, since it is not a function of UAV-related time factors.

The articles in [9]- [13] consider an off-grid UAV-based architecture to serve a set of users with the objective of minimizing the investment cost or maximizing the energy storage. In [9] and [10], the authors minimize the installation cost of a UAV-based cellular network in rural areas while considering UAV recharge over time, coverage, and installation constraints. However, the UAVs hover while serving the users, thereby making the proposed frameworks less efficient. The work in [11] proposes a GA-based solution to maximize the energy stored in UAVs and the ground sites while providing cellular coverage to the considered area; there is no attempt to minimize the investment cost. The authors of [12] propose an energy-efficient mission planning for a UAV-based cellular network to minimize the energy consumed by UAVs and ensure cellular coverage to the users. However, [12] does not consider the power constraints related to the recharging sites. Moreover, it uses the results of [10] to design the energy systems of the UAV recharging sites. [13] proposes an optimization framework to minimize the financial cost of a PV-battery-powered off-grid UAV-based cellular telecommunication network by sizing the energy system using the derived power consumption profiles for three recharging sites. The work uses the results of optimal mission planning in [12] as input to obtain the load profile of each recharging site. However, for real-world IoT applications, the mission planning of the UAVs and the design of the energy system should be investigated as a united problem.

The work in [14] - [26] consider efficient deployment of UAV-based systems to maximize performance metrics such as coverage area, number of covered users, sum rate, and energy efficiency. The placement optimization of a UAV-based communication system can be generally divided into two categories: quasi-stationary deployment and optimal trajectory design. The first scenario determines optimal hovering position(s) of UAV(s) [14] - [19]; in the second scenario, a set of UAVs move along a designed path that maximizes the considered performance metric [20] - [26]. The authors of [14] and [15] use analytical tools to maximize the coverage region of a UAV-based system by varying the altitude of the UAV. In [16] and [17], the authors use circle packing-based algorithms for the optimal quasi-stationary deployment of a multi-UAV system to maximize the global energy efficiency and throughput, respectively. In [18] and [19], the authors provide multi-UAV deployment strategies based on the K-mean and mean-shift algorithms to maximize the coverage region and the minimum achievable rate, respectively. The authors of [20] and [21] design a UAV-enabled system based on covert wireless communications to enable the ground users to hide their transmissions from each other while conveying critical information to the UAV. The work in [20] uses a penalty successive convex approximation (P-SCA) scheme to jointly design the UAV trajectory and its maximum transmit power of the artificial noise (AN), together with the user scheduling strategy subject to covertness constraint, whereas, [21] uses a heuristic approach to optimize the flying location and transmit power. The trajectory design or placement methods proposed in [20] - [25] formulate the problem to either maximize the energy efficiency or throughput as a mixed-integer non-linear problem (MINLP). This is then solved using the sequential convex programming technique. A comprehensive list of papers that consider UAV placement optimization is available in [26].

B. Major contributions and paper structure

The work in [3] - [8] consider supplying the power required by a fixed base station using PV and battery storage systems. The load to the energy system is modeled as a function of the traffic demand of the base station. However, the load to the CS in a UAV-based architecture is a function of the service demand of the users, as well as the trajectory of the UAV. Although the works [9]- [13] tackle the cost minimization of a UAV-based architecture, they consider a simple hovering UAV scenario. These are sub-optimal solutions for an IoT application since they do not exploit the mobility of UAVs as a tool to minimize the cost by reducing both their number and the load to the CS. Moreover, the load profiles do not present an interactive formulation that allows us to show its response to the mission and UAV-related time factors, such as the delay between the successive data harvesting from a node, active and charging time of a UAV, etc. Coverage and energy-efficient UAV deployment strategies are proposed in [14]- [26]. However, the authors do not consider the presence of a ground CS, and all the missions are set to have a duration less than or equal to the active time of a UAV. The objectives are either to determine an optimal altitude that maximizes the coverage area or to find the trajectory parameters that maximize the number of bits transmitted per Joule of Energy consumed. Maximizing the coverage area/ energy efficiency might not always minimize the cost. For instance, the energy efficiency can be improved by flying the AAP at an optimal velocity which is not equal to the maximum velocity. This increases the delay, which forces the system to deploy another AAP if the delay in visiting the same user in succession is greater than the network's time difference of arrival (TDOA), thereby increasing the cost. Therefore the trajectory design to minimize the cost requires further attention. In this work, the objective of cost-efficient design and deployment of a UAV-based system in areas without access to a reliable electricity grid is pursued. The major contributions of this paper can be summarized as follows:

- Proposing a novel wave-based method to generate the load profile of a CS in an EN UAV-based mobile network as a function of the number of AAPs and its mission parameters.
- Designing an efficient AAP path design based on the mean-shift algorithm that minimizes the number of AAPs subject to data harvesting and trajectory constraints. This method makes it possible to solve the problem using convex optimization techniques and can be tweaked to optimize any performance metric.

- Employing the above to minimize the overall cost of deploying an EN UAV-based communication network that harvests data from a set of IoT nodes over set intervals of time.

Section II describes the considered scenario and the applied models. Section III illustrates the problem formulation and the wave-based load profile modeling, as well as the mean-shift clustering-based trajectory design. The main findings of this paper are summarized in Section IV.

II. System Model and Definitions

In this work, a delay-tolerant IoT network is considered, in which a UAV-based EN system is deployed to collect Q bits of data from a set of ground users (GUs) every T_{period} seconds. In practice, T_{period} is the time difference of arrival (TDOA) of the IoT network, and is a function of the memory capacity of the IoT sensor nodes. The EN system, as shown in Fig. 1, consists of a flock of AAPs, and a CS on the ground to harvest and store the required energy for the AAPs. The CS is formed by two elements:

- an energy harvesting PV system, consisting of a number N_{pv} of solar panels, each of cost C_{pv} €, that harvest energy from solar irradiation;
- a battery unit of N_{bt} units, each costing C_{bt} €, to store the energy harvested in surplus and use it to supplement the PV module when this cannot sustain the load by itself.

A flying AAP is called *active* AAP, whereas one at the CS, either charging or waiting to be deployed, is called *idle* AAP. The system is assumed to work for an amount of time T_{service}, measured in hours, within a given time slot of a day: $\mathcal{T} \equiv [T_{\text{start}}, T_{\text{start}} + T_{\text{service}}]$, where T_{start} is the time of the day, thus ranging from from 00:00 hrs to $(24{:}00 - T_{\text{service}})$ hrs. For tractability, the trajectory of the AAP corresponding to one data harvesting cycle is divided into R path segments, represented using $R+1$ waypoints [23]. The length of each segment is constrained to be small enough as to assume the channels between the AAP and each GU to remain stationary:

$$\left\|\mathbf{r}_{\text{h},r+1} - \mathbf{r}_{\text{h},r}\right\| \leq \min\left\{\delta, T_r \cdot v_{\max}\right\} \ \forall r \in \mathcal{R} = \{1, 2, ..R\} \quad (1)$$

where δ is chosen so that, within each path segment, the AAP can be assumed to either hover or fly at a constant velocity v_r, which cannot be higher than the maximum AAP velocity $v_{\max}$. $\mathbf{r}_{\text{h},r} = (x_r, y_r)$ represents the horizontal-plane coordinates of the 3D position of the r^{th} path segment of the AAP $\mathbf{r}_r = (\mathbf{r}_{\text{h},r}, \mathbf{r}_{\text{v},r})$, in which $r_{\text{v},r}$ corresponds to the vertical coordinate of the AAP; the AAP is assumed to fly at a constant altitude: $r_{\text{v},r} = h_{\text{a}} \forall r \in \mathcal{R}$. The AAP schedules one GU at a time for data uplinking, thereby following a time division multiple access (TDMA) scheme to serve the GUs. If T_r is the time that the AAP spends in the r^{th} path segment, and $T_{n,r}$ is the time allocated to the n^{th} GU when the AAP is in the r^{th} path segment, then $T_{\text{Hcycle}} = \sum_{r=1}^{R} T_r$ is the time it takes the AAP to harvest Q bits of data from N GUs such that,

$$\sum_{n=1}^{N} T_{n,r} \leq T_r \qquad \forall r \in \mathcal{R}. \quad (2)$$

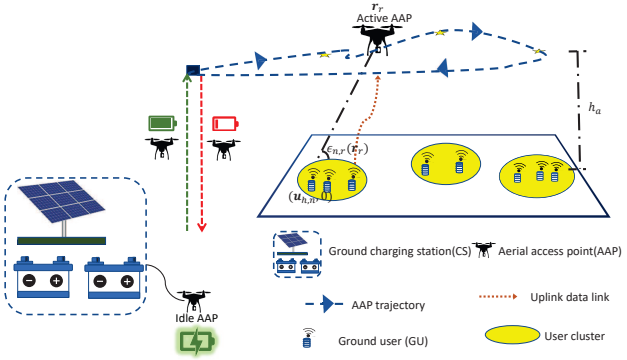

Figure 1: Considered application scenario: the AAP(s) is (are) deployed to collect data from a set of ground IoT nodes; an active AAP with little energy left is replaced by a fully charged idle AAP.

Also, the n^{th} GU is located at ground level with the corresponding horizontal plane coordinates $\mathbf{u}_{\text{h},n} = (x_n, y_n) \forall n \in \mathcal{N} = \{1, 2, ..N\}$.

A. How is data harvested from the GUs?

At T_{start}, a fully charged AAP ascends from the CS and follows the optimal trajectory (designed as explained in Section III-B). If the time it takes the AAP to complete one cycle of data harvesting is greater than the TDOA of the network ($T_{\text{Hcycle}} > T_{\text{period}}$), then a second AAP from the ground station is deployed at $T_{\text{start}} + (T_{\text{period}}/3600)$ hours, following the same trajectory as that of the previously deployed AAP[1]. This data harvesting cycle continues for T_{service} hrs. The AAPs are assumed to be operating in orthogonal frequency bands to minimize the inter-user interference (e.g., narrowband frequency division multiple access systems [34]). The frequency reuse technique used in the conventional fixed-telecommunication system can be used to accommodate any number of AAPs without increasing the available bandwidth. Additionally, at the beginning of each cycle of data harvesting, the on-board battery of the AAP is checked to guarantee that it has enough energy to complete the cycle; if not, it returns to the CS for recharging, and it is replaced by a fully recharged AAP, as shown in Fig. 1.

B. Propagation Environment

The communication channel between the AAP and a GU can be either line-of-sight (LoS) or non-LoS (NLoS), depending on the relative position of the GU with respect to the AAP and the building profile of the region [14]- [25]. Hence, the probability of having a LoS channel between the n^{th} GU and the AAP while the AAP is in the r^{th} path segment is determined using,

$$\mathbb{P}_{n,r}^{\text{los}}(\mathbf{r}_r) = \frac{1}{1 + a \cdot \exp\left\{-b \cdot [\epsilon_{n,r}(\mathbf{r}_r) - a)]\right\}}, \quad (3)$$

where a, b are the environment-dependent parameters that are fundamentally decided by the building profile of the region [14], and $\epsilon_{n,r}(\mathbf{r}_r) = (180/\pi)\tan^{-1}\left[\frac{h_{\text{a}}}{\|\mathbf{r}_{\text{h},r} - \mathbf{u}_{\text{h},n}\|}\right]$ is the

[1]In this work, we are not considering the case $T_{\text{period}} = 0$; when $T_{\text{period}} = 0$, a suitable aerial cell planning is required to minimize the number of AAPs, as proposed in [17] and [25].

corresponding elevation angle. The LoS and NLoS path loss values in dB are expressed as [14], [17], [25], ,

$$L^{\mathrm{g}}_{n,r}(\mathbf{r}_r) = 20\cdot\log d_{n,r}(\mathbf{r}_r) + 20\cdot\log f + 20\cdot\log\left(\frac{4\pi}{v_{\mathrm{light}}}\right) + \eta^{\mathrm{g}} \quad (4)$$

where $g \in \{\mathrm{los}, \mathrm{nlos}\}$, $d_{n,r}(\mathbf{r}_r) = \sqrt{\|\mathbf{r}_{\mathrm{h},r} - \mathbf{u}_{\mathrm{h},n}\|^2 + h_{\mathrm{a}^2}}$; f and v_{light} are the respective signal frequency and the velocity of light; η^{los} and η^{nlos} are the mean values of the additional path loss for LoS and NLoS links due to the environment, respectively. For a given elevation angle, this additional loss has a Gaussian distribution [27], and it depends on the building profile of the region. However, from [27], it is noticed that the change in the additional path loss within a particular propagation group (LoS/NLoS) is insignificant compared to the change in path loss value from one group to the other: the NLoS path loss value depends on the scattering and reflections from the surrounding buildings which depend largely on the frequency of operation and the building profile of the region rather than the distance. This allows us to model the path loss with a constant gap between the two propagation groups. Consequently, the average amount of exchanged data in bits-per-seconds-per-Hertz (bps/Hz) is given by,

$$D_{n,r}(\mathbf{r}_r) = \mathbb{P}^{\mathrm{los}}_{n,r}(\mathbf{r}_r)\log_2\left(1 + \frac{P}{\sigma^2 10^{L^{\mathrm{los}}_{n,r}(\mathbf{r}_r)/10}}\right) + \mathbb{P}^{\mathrm{nlos}}_{n,r}(\mathbf{r}_r)\log_2\left(1 + \frac{P}{\sigma^2 10^{L^{\mathrm{nlos}}_{n,r}(\mathbf{r}_r)/10}}\right), \quad (5)$$

where $\mathbb{P}^{\mathrm{nlos}}_{n,r}(\mathbf{r}_r) = 1 - \mathbb{P}^{\mathrm{los}}_{n,r}(\mathbf{r}_r)$, and P and σ^2 are the signal and noise power, respectively. The principal reason for considering a probabilistic LoS-NLoS air to ground channel model is the lack of the building map of the region. If the building map of the region is available, the value of $\mathbb{P}^{\mathrm{los}}_{n,r}(\mathbf{r}_r)$ can be determined using ray tracing methods, and (5) can be modified accordingly. Hence, the mean shift clustering-based trajectory design we propose in Section III-B can be used for several scenarios, including a channel estimated using a deep neural network [28].

C. UAV Power consumption Model

In the considered system, the AAP takes off vertically from the CS to replace an out-of-power AAP, then the latter descends vertically for recharging; during data harvesting, the AAP flies horizontally or hovers to collect the data from the users. The total power consumption of the AAP is the sum of the power consumed by the UAV and the radio access node; since the power consumed by the radio access node is negligible compared that consumed by the UAV (by two orders of magnitude) [17], [23], it is assumed that the power consumption of the whole AAP is equal to that of the UAV. The UAV parameters are summarized in Table I. From [25], the power required by the AAP for flying horizontally and vertically is given by (6) and (7), respectively:

$$P_{\mathrm{h}}(v_r) = \underbrace{N_{\mathrm{rotor}}P_{\mathrm{b}}\left(1 + \frac{3v_r^2}{v_{\mathrm{tip}}^2}\right)}_{P_{\mathrm{blade}}} + \underbrace{\frac{1}{2}U_{\mathrm{d}}A_{\mathrm{f}}\rho(h_{\mathrm{a}})v_r^3}_{P_{\mathrm{fuselage}}} + \underbrace{W\left(\sqrt{\frac{W^2}{4N^2_{\mathrm{rotor}}\rho^2(h_{\mathrm{a}})A^2_{\mathrm{rotor}}} + \frac{v_r^4}{4}} - \frac{v_r^2}{2}\right)^{1/2}}_{P_{\mathrm{induce}}}, \quad (6)$$

$$P_{\mathrm{v}}(v_{\mathrm{c}}) = \frac{W}{2}\left(v_{\mathrm{c}} + \sqrt{v_{\mathrm{c}}^2 + \frac{2W}{N_{\mathrm{rotor}}\rho(h_{\mathrm{a}})A_{\mathrm{rotor}}}}\right) + N_{\mathrm{rotor}}P_{\mathrm{b}}. \quad (7)$$

where $P_{\mathrm{b}} = \frac{\Delta}{8}\rho(h_{\mathrm{a}})sA_{\mathrm{rotor}}v_{\mathrm{tip}}^3$, $\rho(h_{\mathrm{a}}) = (1 - 2.2558.10^{-5}h_{\mathrm{a}})^{4.2577}$. P_{blade} and P_{fuselage} are the power levels required to overcome, respectively, the profile drag forces of the rotor blades and the fuselage of the aerial vehicle opposite to its forward movement; P_{induce} represents the power required to lift the payload. Replacing $v_r = 0$ in (6) gives the power level required for hovering.

D. PV-battery system modeling

1) PV modeling

The considered model for the PV power generation has the following expression:

$$P_{\mathrm{pv}}(N_{\mathrm{pv}}, t) = I_{\mathrm{irr}}(t)\cdot A_{\mathrm{pv}}\cdot N_{\mathrm{pv}}\cdot\eta_{\mathrm{pv}}, \quad (8)$$

where $I_{\mathrm{irr}}(t)$ is the solar irradiance at time t on a south-oriented plane with tilt angle of 30°, measured in W/m^2; A_{pv} is the panel area (m^2), and η_{pv} is the panel efficiency (assumed constant).

2) Ground battery modeling

Battery storage devices are combined with RESs, such as PV panels, to offset the intermittency of these resources. The power needed by the CS to recharge the AAPs is supplied by either the PV panels or the ground battery, depending on the availability of the solar energy. If there is a surplus of power generation, the extra power is redirected towards recharging the batteries of the charging station, as long as their capacity allows it. If, on the other hand, the power generation is not sufficient, the remaining power is drawn from the ground battery. The battery model, including its boundary conditions, is adapted from that in [32], and it is the following:

$$E_{\mathrm{bt}}(t) = E_{\mathrm{bt}}(t-\Delta t) + P_{\mathrm{bt}}(t)\cdot\Delta t\cdot\eta_{\mathrm{bt}}(P_{\mathrm{bt}}) \quad (9a)$$

$$E_{\mathrm{bt}}(0) = N_{\mathrm{bt}}\beta_{\mathrm{module}}\mathrm{SOC}_{\max}, \quad (9b)$$

$$N_{\mathrm{bt}}\beta_{\mathrm{module}}\mathrm{SOC}_{\min} \le E_{\mathrm{bt}}(t) \le N_{\mathrm{bt}}\beta_{\mathrm{module}}\mathrm{SOC}_{\max} \quad (9c)$$

$$P_{\mathrm{bt}}(t) \le P_{\mathrm{Ch,max}}, \quad \text{when } P_{\mathrm{bt}}(t) > 0 \quad (9d)$$

$$|P_{\mathrm{bt}}(t)| \le P_{\mathrm{DCh,max}}, \quad \text{when } P_{\mathrm{bt}}(t) < 0, \quad (9e)$$

where $E_{\mathrm{bt}}(t)$ is the energy stored in the battery at time t; $P_{\mathrm{bt}}(t)$ is the power flowing into the battery (negative when the battery is discharging); Δt is the time interval considered, and $\eta_{\mathrm{bt}}(P_{\mathrm{bt}})$ is the battery efficiency, which depends on the sign of P_{bt} because charging and discharging efficiencies are different. As per the constraints, N_{bt} is the number of battery modules, β_{module} is the capacity of one battery module, $\mathrm{SOC}_{\min}$ and $\mathrm{SOC}_{\max}$ are the minimum and maximum State-of-Charge (SOC) of the battery, which indicates the level of charge relative to the capacity. Hence, conditions (9b) and (9c) mean that the battery pack is initially fully charged, ($\mathrm{SOC} = \mathrm{SOC}_{\max}$), while the battery is considered depleted

Table I: UAV Parameters [25].

Label	Definition	Value	Label	Definition	Value
W	Weight of the UAV	32.34 N	$\rho(h_a)$	Air density	-
N_{rotor}	Number of rotors	4	U_{d}	Drag coefficient	0.9
v_r	UAV's horizontal flying velocity	-	A_{rotor}	Rotor disc area	0.06 m^2
Δ	Profile drag coefficient	0.002	v_{tip}	Tip speed of the rotor	102 m/s
s	Rotor solidity	0.05	A_{f}	Fuselage area	0.038 m^2
v_{c}	ascent/descent velocity	5 m/s			

when $\text{SOC} = \text{SOC}_{\min}$. Finally, (9d) and (9e) impose maximum input and output powers, as specified in the battery datasheet.

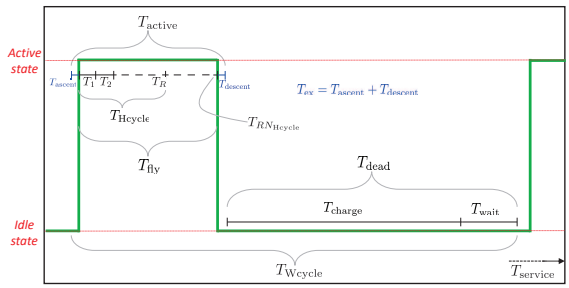

Figure 2: Time components of an AAP work cycle.

E. AAP mission breakdown

The time intervals that define the work cycle of an AAP during a mission are displayed in Fig. 2, and are defined as follows:

- T_{active} is the active time of an AAP, i.e., the total time it spends flying before recharging. T_{active} is given by the sum of the horizontal flying time T_{fly} and the exchange time T_{ex}:
$$T_{\text{active}} = \underbrace{N_{\text{Hcycle}} \cdot T_{\text{Hcycle}}}_{T_{\text{fly}}} + \underbrace{T_{\text{descent}} + T_{\text{ascent}}}_{T_{\text{ex}}}, \quad (10)$$
where T_{fly} is the product of the duration of a cycle of data harvesting and the number of cycles, N_{Hcycle}, an AAP can withstand before running out of energy; T_{ex} is the time spent in the exchange process, from when the substitute AAP leaves the CS to when the discharged AAP reaches the CS. It is obtained by summing the descent and ascent times, T_{descent} and T_{ascent}, which are, respectively, the time an AAP needs to return to and to leave the CS.
- T_{charge} is the time needed to fully recharge an AAP, which is calculated based on the capacity of each AAP's on-board battery β_{aap}, its Depth-of-Discharge DOD_{aap} (the proportion of capacity that is used during each work cycle), and its average charging power P_{charge}:
$$T_{\text{charge}} = \beta_{\text{aap}} \text{DOD}_{\text{aap}} P_{\text{charge}}. \quad (11)$$
- T_{wait} is the interval in which an AAP is charged, but it is waiting for the an active AAP to finish its mission before being deployed. Its value is determined by using the two definitions of T_{Wcycle}, one referring to a single AAP, and the other to a whole flock, as follows:
$$\begin{aligned} T_{\text{Wcycle}} &= T_{\text{active}} + T_{\text{charge}} + T_{\text{wait}} \\ &= N_{\text{aap}} \left(T_{\text{active}} - \frac{T_{\text{ex}}}{2} \right) \end{aligned}$$
$$\rightarrow T_{\text{wait}} = (N_{\text{aap}} - 1) T_{\text{active}} - T_{\text{charge}} - N_{\text{aap}} \frac{T_{\text{ex}}}{2}. \quad (12)$$
- The period T_{Wcycle} is the interval corresponding to a full AAP work cycle, given by the sum of the time the AAP spends in each of the three states: active, charging, and idle,
$$T_{\text{Wcycle}} = T_{\text{active}} + T_{\text{charge}} + T_{\text{wait}}. \quad (13)$$

III. Optimal Design of an Energy-Neutral System

In this section, it is explained how a cost-efficient EN system is achieved by optimally designing the trajectory of the AAP and efficiently selecting the configuration of the CS. The corresponding optimization problem can be formulated as,

$$\begin{aligned} (\text{P1}): \underset{\substack{\text{N}_{\text{pv}}, N_{\text{bt}}, \{\mathbf{r}_r\}, \\ \{\text{T}_r\}, \{T_{n,r}\}}}{\text{minimize}} \quad & C_{\text{inv}} \left[N_{\text{pv}}, N_{\text{bt}}, N_{\text{aap}}(\{T_r\}) \right], & (14a) \\ & P_{\text{pv}}(N_{\text{pv}}, t) + P_{\text{bt}}(N_{\text{bt}}, t)\eta_{\text{bt}} \\ & \quad \geq P_{\text{ld}} \left[N_{\text{aap}}(\{T_r\}), t \right], \forall t, & (14b) \\ & \frac{\delta}{T_r} \leq v_{\max} \qquad \forall r & (14c) \\ & \sum_{r=1}^{R} T_{n,r} B D_{n,r}(\mathbf{r}_r) \geq Q \quad \forall n, & (14d) \\ & \mathbf{r}_{\text{h},1} = \mathbf{r}_{\text{h},c(R+1)} = \mathbf{r}_{\text{CS}}, \forall c \in \{1, 2, ..., N_{\text{Hcycle}}\}, & (14e) \\ & (1), (2), (8) - (9e). & (14f) \end{aligned}$$

The objective function of (P1) is the total investment cost, consisting in the costs of the PV panels, battery units, and the AAPs:

$$\begin{aligned} C_{\text{inv}}(N_{\text{pv}}, N_{\text{bt}}, N_{\text{aap}}(\{T_r\})) &= N_{\text{pv}} C_{\text{pv}} + N_{\text{bt}} C_{\text{bt}} \\ &\quad + N_{\text{aap}}(\{T_r\}) C_{\text{aap}}, \quad (15) \end{aligned}$$

where $N_{\text{aap}}(\{T_r\})$ is the total number of AAPs, each costing C_{aap} €; $N_{\text{aap}}(\{T_r\})$ is the sum of idle and active AAPs, where the number of active AAPs is determined by the TDOA of the network T_{period} and the time it takes an AAP to complete one cycle of data harvesting:

$$N_{\text{active}}(\{T_r\}) = \left\lceil \frac{\sum_{r=1}^{R} T_r}{T_{\text{period}}} \right\rceil, \quad (16)$$

where $\lceil x \rceil$ rounds x to the nearest integer greater than or equal to x. Therefore, the total number of AAPs required to guarantee that there is always a fully charged AAP ready to be deployed to replace a depleted AAP is determined as [25],

$$N_{\text{aap}}(\{T_r\}) = \left\lceil \left(\frac{T_{\text{dead}}}{T_{\text{active}}} + 1 \right) N_{\text{active}}(\{T_r\}) \right\rceil, \quad (17)$$

with T_{dead} defined as the sum of charging and wait times, $T_{\text{dead}} = T_{\text{charge}} + T_{\text{wait}}$. T_{active} is obtained from the data-

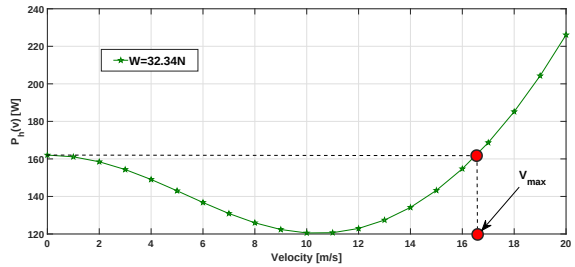

Figure 3: UAV power consumption as a function of the velocity.

sheet [2] of the UAV used. Usually, the UAV manufacturers specify T_{active} as the hovering time for a given payload. Since the hovering power is greater than the horizontal flying power of the UAV until a particular velocity value, the maximum AAPs flying speed is set to be $v_{\max}$ in (14c), where $v_{\max}$ is obtained from the power profile of the AAP, as shown in Fig. 3. This ensures that T_{active} will be greater than or equal to the hovering time indicated in the data-sheet. The corresponding number of idle AAPs is then determined as $N_{\text{idle}}(\{T_r\}) = N_{\text{aap}}(\{T_r\}) - N_{\text{active}}(\{T_r\})$. Constraint (14b) is the energy neutrality constraint, which guarantees that the CS load power requirement is always satisfied, regardless of whether power is provided by the PV panels or the ground battery. One of the challenges in solving (P1) is the difficulty in representing the load to the CS at a given time t as a function of T_{period}, T_{Hcycle}, T_{active}, and T_{dead}. In Section III-A, a novel model is developed to represent the load, $P_{\text{ld}}\left[N_{\text{aap}}(\{T_r\}), t\right]$, as a function of the number of AAPs. Eq. (14d) guarantees the delivery of Q bits of data from all the GUs to the AAP within T_{Hcycle} s, with B being the available bandwidth. Eq. (14e) ensures that each data harvesting cycle starts and ends above the charging station location, $\mathbf{r}_{\text{CS}}$.

A. Wave-based load profile modeling of the CS

From the point of view of the CS, an AAP can only be in two alternative states: charging or not charging. In the previously described scenario, these two states will periodically repeat themselves within a given period of time. Let, $K_{\text{aap},i}(t)$ be the function describing the state of the i^{th} AAP at time t, such that:

$$K_{\text{aap},i}(t) \equiv \begin{cases} = 0, & \text{when AAP starts/stops charging;} \quad (18a) \\ > 0, & \text{when AAP is charging;} \quad (18b) \\ < 0, & \text{when AAP is not charging;} \quad (18c) \\ & \text{is periodical with period } T_{\text{Wcycle}}. \quad (18d) \end{cases}$$

The above conditions can be met by modeling $K_{\text{aap},i}(t)$ as a function of the following variables:

$$K_{\text{aap},i}(t) = F\left(T_{\text{period}}, T_{\text{Wcycle}}, T_{\text{Hcycle}}, T_{\text{active}}, T_{\text{charge}}\right). \quad (19)$$

The solution to model F, inspired by the modulation of power electronics, is to use a sinusoidal function that can be converted into a square wave at a later stage, using a comparative function. This approach allows synthetic expression for whatever number of cycles and even AAPs, and it is easy to implement in any programming language. Its expression is the following:

$$K_{\text{aap},i}(t) = \alpha \sin\left\{\omega(T_{\text{Wcycle}})\left[t + \phi(T_{\text{active}}, T_{\text{charge}}) - \zeta_i(T_{\text{Hcycle}}, T_{\text{period}}) + \gamma(T_{\text{Wcycle}}, T_{\text{charge}}).\right.\right. \quad (20)$$

In order to meet the conditions described in (18a)-(18d), the shape of (20) can be adjusted by tweaking its five coefficients, as follows:

- α is the amplitude of the wave, but in this case it is only used to specify the sign of the function. Its value is $\alpha = -1$ if the cycle starts with an already charged AAP (or vice-versa);
- $\omega(T_{\text{Wcycle}})$ is the period of the sine wave, which can be calculated as $\omega(T_{\text{Wcycle}}) = \frac{2\pi}{T_{\text{Wcycle}}}$, as a consequence of the definition of period applied to condition (18d);
- $\phi(T_{\text{active}}, T_{\text{charge}})$ is the phase of the wave, which establishes the shape of the function. It is found by imposing (18a) at $t = T_{\text{active}}$ and $t = T_{\text{active}} + T_{\text{charge}}$, resulting in $\phi(T_{\text{active}}, T_{\text{charge}}) = \frac{\arcsin\left(-\frac{C}{A}\right)}{\omega} - T_{\text{active}}$;
- $\zeta_i(T_{\text{Hcycle}}, T_{\text{period}})$ is the delay between the launch of the first and the i^{th} AAP, as explained in Section II-A:

$$\zeta_i(T_{\text{Hcycle}}, T_{\text{period}}) = \begin{cases} 0 & \text{if} \quad i = 1 \\ (i-1) \cdot \frac{T_{\text{period}}}{\left\lceil \frac{T_{\text{Hcycle}}}{T_{\text{period}}} \right\rceil}, & \text{if} \quad \begin{matrix} \text{T}_{\text{Hcycle}} \geq T_{\text{period}}, \\ \forall i \in \{2, 3, .., N_{\text{aap}}(\{T_r\})\} \end{matrix} \\ T_{\text{active}}, & \text{if} \quad T_{\text{Hcycle}} < T_{\text{period}}. \end{cases} \quad (21)$$

- $\gamma(T_{\text{Wcycle}}, T_{\text{charge}})$ is a constant that can shift the wave upwards or downwards without affecting its shape. For $\gamma(T_{\text{Wcycle}}, T_{\text{charge}}) = 0$, the ratio between T_{charge} and T_{Wcycle} would be 0.5, while for $\gamma(T_{\text{Wcycle}}, T_{\text{charge}}) = 1$ the AAP would be charging the whole time. Thus, the general formulation is $\gamma(T_{\text{Wcycle}}, T_{\text{charge}}) = \frac{T_{\text{charge}}}{2T_{\text{Wcycle}}} - 1$.

Now, all the cycle functions $K_{\text{aap},i}(t)$ are transformed into state functions $S_{\text{aap,i}}(t)$ of value 1 when the AAP is charging, 0 when it is not, consistently with the convention adopted initially:

$$S_{\text{aap},i}(t) = \begin{cases} 1, & \text{if} \quad K_{\text{aap},i}(t) > 0, \\ 0, & \text{if} \quad K_{\text{aap},i}(t) \leq 0. \end{cases} \quad (22)$$

Then, the sum of all the state functions S_{aap} provides the number of AAPs recharging at the same time:

$$\text{ld}\left[N_{\text{aap}}(\{T_r\}), t\right] = \sum_{i=1}^{N_{\text{aap}}(\{T_r\})} S_{\text{aap},i}(t). \quad (23)$$

The resulting curves are visualised in Fig. 4, where three AAP curves exemplify two cases: one where a single active AAP is enough to satisfy the delay constraint, and one where at least two AAPs must be active at the same time. It is shown in grey the load function defined by (23), i.e., the number of AAPs connected to the CS at any given time. It can be observed how the steps of the load function correspond with the intersection between a state function K and the $\text{Time} = 0$ axis. Finally, the load on the CS can be calculated by multiplying the number of charging AAPs by the power consumed to charge a single

[2]https://dl.djicdn.com/downloads/m100/M100_User_Manual_EN.pdf

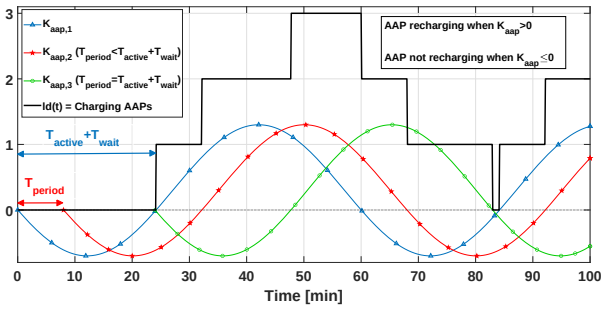

Figure 4: Visualization of three AAP state functions, and the consequent load on the charging station.

AAP, $\frac{P_{\text{charge}}}{\eta_{\text{aap}}}$. Hence, the RHS of (14b) becomes:

$$P_{\text{ld}}\left[N_{\text{aap}}(\{T_r\}),t\right] = \frac{P_{\text{charge}}}{\eta_{\text{aap}}} \cdot \text{ld}\left[N_{\text{aap}}(\{T_r\}),t\right] + \Psi(t). \quad (24)$$

The function Ψ represents the power consumption associated with recalculating the optimal trajectory locally, a binary function assuming the value of computational power when the computation is executed, and zero at all other times. Since the charging power was assumed to be a constant, $P_{\text{ld}}\left[N_{\text{aap}}(\{T_r\}),t\right]$ will have the same shape as $\text{ld}\left[N_{\text{aap}}(\{T_r\}),t\right]$, but it will be expressed in Watts. For a given T_{period}, from (14b), the number of required PV panels and battery units is proportional to the load profile on the CS; from (24), the load profile of the CS is in turn a function of the number of AAPs. Therefore, the size of the AAP fleet has an impact on the number of PV panels and battery units. Thus, from (14b) and (24), minimizing the number of AAPs means minimizing the objective function of (P1). Once the minimum number of AAPs required to harvest Q bits of data from N GUs within T_{period} is determined, the cost-efficient combination of PV panels and battery units is directly consequential.

B. Minimum number of AAPs

In this section we design a trajectory that minimizes the number of AAPs required to harvest data from the GUs every T_{period} during T_{service}. The corresponding problem is formulated as,

$$\text{(P1.1)}: \underset{\{\mathbf{r}_r\},\{T_{n,r}\},\{T_r\}}{\text{minimize}} \quad N_{\text{aap}}(\{T_r\}), \quad (25a)$$

$$N_{\text{aap}}(\{T_r\}) \geq \left(\frac{T_{\text{dead}}}{T_{\text{active}}} + 1\right) N_{\text{active}}(\{T_r\}) \quad (25b)$$

$$N_{\text{active}}(\{T_r\}) \geq \frac{\sum_{r=1}^{r} T_r}{T_{\text{period}}} \quad (25c)$$

$$(1), (14c) - (14e). \quad (25d)$$

In (P1.1), we have relaxed the integer constraint on the number of active and total AAPs. After determining the trajectory variables, the values will be rounded to the nearest greater integer. (P1.2) is a non-convex optimization problem due to the non-convex form of $D_{n,r}(\mathbf{r}_r)$, used in (14d). Hence, the solution is found by dividing the problem into two sub-problems: 1) AAP path design using mean-shift clustering; 2) update of $\{T_r\}$ and $\{T_{n,r}\}$ for the obtained AAP path.

In practice, the number of GUs is large, or they are likely to form clusters. Thus, to find the cluster properties of user distributions, one can exploit the mean-shift algorithm proposed in [19] to identify the locations with the highest density of users. When the number of users is high, the cluster centers are potential points for the AAP trajectory. In addition, in cases where the users form clusters in advance, such as in rural areas, referring to these centers prevents the AAP from visiting locations where there are no GUs. The cluster centers obtained from Algorithm 1 of [19] are the potential points through which the AAP must pass. Since the active number of AAPs can be reduced by minimizing $\sum_{r=1}^{R} T_r$, the shortest path between the potential points is determined using the traveling salesman algorithm [30]. The resulting continuous path between cluster centers is then discretized into small segments, each of length δ, satisfying constraint (1), and providing the set of waypoints $\{\mathbf{r}_r\}$. The values of $D_{n,r}(\mathbf{r}_r)$ are then calculated using (5). The scheduling problem now takes the following form:

$$\text{(P1.2)}: \underset{\{T_{n,r}\},\{T_r\}}{\text{minimize}} \quad N_{\text{aap}}(\{T_r\}), \quad (26a)$$

$$(14c) - (14e), (25b), (25c) \quad (26b)$$

Problem (P1.2) is a convex optimization problem, and can be solved with solvers like CVX.

C. Cost-efficient CS design

In the previous section, the load to the CS was represented as a function of the number of AAPs. Also, a trajectory was found that minimizes the number of AAPs, thereby minimizing the load on the CS and the economic impact of purchasing AAPs. In this section, efforts are directed towards minimizing the number of PV panels and ground battery units of the CS, N_{pv} and N_{bt}, while satisfying the power requirement of the CS. The corresponding problem is formulated as,

$$\text{(P1.3)}: \underset{N_{\text{pv}},N_{\text{bt}}}{\text{minimize}} \quad C_{\text{inv}}\left[N_{\text{pv}}, N_{\text{bt}}, N_{\text{aap}}(\{T_r\})\right], \quad (27a)$$

$$P_{\text{pv}}(N_{\text{pv}},t) + P_{\text{DCh}}(N_{\text{bt}},t)\eta_{\text{bt}} \geq P_{\text{ld}}\left[N_{\text{aap}}(\{T_r\}),t\right], \forall t, \quad (27b)$$

$$(8) - (9e). \quad (27c)$$

1) Constrained search algorithm

The constrained search algorithm proposed to solve (P 1.3) is an enhanced version of a classic 'brute force' algorithm. Brute force methods, also known as exhaustive search, offer a forthright and very accurate optimization approach of solving problems, visiting all possible search points in the design space, in order to find the global optimum within a given search space [33].Their main drawback is the high computational load, but, in the present application, this is acceptable due to the simple form of problem (P1.3). Since the trajectory optimization is now decoupled from the CS design, this can be carried out by manipulating only two variables: N_{pv} and N_{bt}. With a classic extensive search, all the solutions generated from the combination of these two variables would be simulated to evaluate their cost and power profile. The ones not satisfying constraint (27b) would be simply discarded, and the remaining ones compared by their cost to find the global minimum. However, the constrained search algorithm achieves the same result with less iterations: for each number of PV panels, the size of the battery is progressively increased until

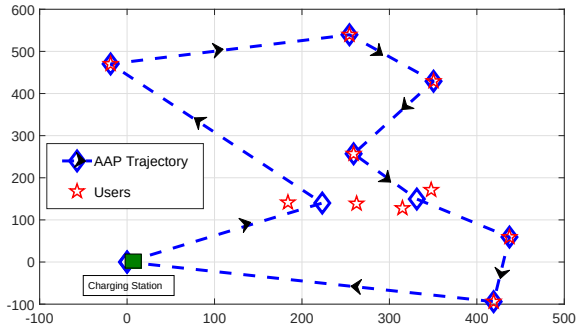

Figure 5: Horizontal projection of a sample AAP trajectory to collect 200 Mbits of data from 10 randomly distributed users.

the condition posed by constraint (27b) is met. This skips the simulation of several configurations that would be later discarded for their excessive cost. Algorithm 1 summarizes the steps involved in designing a UAV-based cost-efficient EN system to serve a set of IoT ground units.

IV. Results and Discussion

The simulation parameters used to generate the results described in this section are listed in Table II. In Section IV-A, the results related to the trajectory design are discussed, and in Section IV-B the results of the cost-efficient system design are presented.

A. AAP Trajectory

Fig. 5 shows a sample path an AAP follows to collect 200 Mbits of data from a set of 10 users, uniformly distributed over a square region of side 600m. The CS is placed at $(0, 0, 0)$. The set of feasible points the AAP should pass through are determined using the mean-shift algorithm. Fig. 6a and Fig. 6b show the trajectory parameters and the user scheduling obtained by solving (P 1.2); the flying velocity of the AAP in each path segment shows how this AAP trajectory satisfies the maximum velocity constraint (14c); also, by the end of the trajectory, all the users have delivered 200 Mbits of data, thereby satisfying the data harvesting constraint (14d). Moreover, the horizontal projection of the trajectory starts and ends above the CS location (14e). Fig. 7 shows the advantage of the suggested mean-shift method path design when compared to two baseline scenarios:

Algorithm 1: Cost-Efficient EN System Design

1 Initialize the locations of GNs;
2 Find the user-cluster centers using the mean-shift algorithm;
3 Find the shortest path between the centers using the travelling salesman algorithm;
4 Segment the path into R segments of length δ and find $\{D_{n,r}(\mathbf{r}_r)\}$ using (5);
5 Solve (P1.2) to get the trajectory variables, the GU scheduling, and the minimum number of AAPs;
6 Model the load to the CS using (23);
7 Use the constrained search algorithm to find the minimum number of PV and battery units that allows to meet the load requirement.

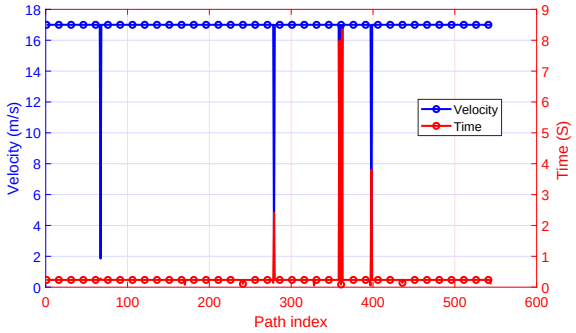

(a) Velocity- Time profile.

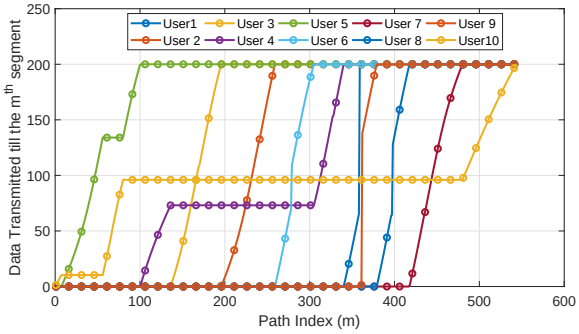

(b) Scheduling

Figure 6: a)The total time and energy to collect the data is 148 seconds; and 6.9133 Wh, respectively; b)AAP collects 200 Mbits of data from all the users by the end of the trajectory.

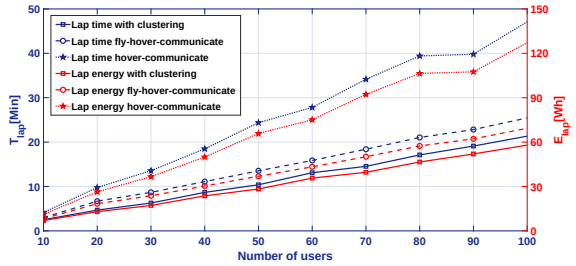

Figure 7: AAP lap time energy consumption: the proposed method versus the baseline scenarios.

1) the AAP flies at its maximum velocity to each user and hovers right on top of it to complete the data transmission. This is widely known as fly-hover-communicate protocol [23], [25];
2) the AAP hovers at the center of the coverage region (hover-communicate) [14], [15].

As seen in Fig. 7, the proposed method outperforms the two baseline scenarios in terms of both time and energy an AAP needs to complete a cycle of data harvesting. The hover-communicate scenario has the worst performance because the mobility of the AAP is not exploited to optimize the channels between AAP and users. The benefits of user clustering are maximized when the number of users is large. Since the expected number of user nodes in an IoT network is very large, the proposed path design is an ideal candidate for an IoT data harvesting application.

B. Charging Station design

This section explains the findings related to the design of the CS using the trajectory information from the previous section.

Table II: Simulation Settings

Label	Definition	Value	Label	Definition	Value
A_{pv}	Area of PV panel	1.63 m^2	η_{pv}	Average efficiency of PV panel	17.1%
β_{module}	Energy capacity of a battery module	37.44 Wh	η_{bt}	Average efficiency of ground battery	90%
SOCmin	Minimum battery State-of-Charge	5%	T_{active}	Active time of an AAP	1320 s
SOCmax	Maximum ground battery State-of-Charge	95%	v_{c}	AAP climbing velocity	5 m/s
β_{aap}	On-board battery capacity of an AAP	100 Wh	P_{charge}	AAP nominal charging power	180 W
DOD_{aap}	Depth-of-Discharge of AAP battery	90%	η_{aap}	Average efficiency of AAP battery	85%
f	Channel carrier frequency	5.8 GHz	Q	Data size	-
B	Channel bandwidth	20 MHz	a	P^{los} Constant for suburban topology	4.88
N_0	Noise spectral power	-174 dBm/Hz	b	P^{nlos} Constant for suburban topology	0.43
v_{max}	AAP's maximum speed	17 m/s	η^{loS}	additional mean path loss for LoS group	0.2
δ	Path discretization interval	1 m	η^{nloS}	additional mean path loss for NLoS group	24
P	Transmission power	23 dBm	h_{a}	Flying altitude of an AAP	50 m

A $T_{\text{period}} = 600$s is considered, resulting in $N_{\text{active}}(\{T_r\}) = 1$ from (16); $T_{\text{dead}} = 600$s, giving $N_{\text{aap}}\{T_r\}) = 3$. The irradiation data used in the simulations is obtained from the online database in [31], which refers to the area of Milan, Italy. This is provided with intervals of one minute, so the irradiation was assumed to stay constant over a single interval. The solar panels[3] considered in this study have a unit price C_{pv} of 129.80€. Each battery unit is represented by a pack of 4 Li-ion cells[4], with a unit cost C_{bt} of 39.59€. The load to the CS corresponding to $N_{\text{aap}}(\{T_r\}) = 3$, $T_{\text{period}} = 2580$s, $T_{\text{Wcycle}} = 3900$s, $T_{\text{Hcycle}} = 148$s, $T_{\text{active}} = 1320$s, and $T_{\text{charge}} = 1800$s is then modeled using the the methodology described in section III-C, and the result is shown in Fig. 8. The cost-efficient PV-battery combination that serves the load while satisfying the battery constraints (9a)- (9e) is determined by solving (P 1.3) with the constrained search algorithm. The effect of the battery constraints can be observed indirectly in Fig. 8, as they produce a slightly over-sized battery, which is not fully exploited, at least on an average day. Fig. 8 shows the operation of the designed CS with $T_{\text{start}} = 11:15$ and $T_{\text{service}} = 2$ hrs: as the irradiation starts to grow, the solar panels begin to generate power, which goes all towards charging the battery, since the load is nil until 11:00, when the optimal trajectory is computed. This process takes one minute using an average laptop with a power consumption of 50 W, and it does not impact the system significantly. After 11:15, when the mission starts, the generated power is not enough to supply the load alone, so the battery kicks in, as the drop in its SOC shows. It can be noticed in Fig. 8 how the power consumption profile actually extends beyond the mission duration T_{service}. This is because it is assumed that the AAPs are fully charged in the morning, so they need to be recharged in the evening. However, this can be done slowly, so as to avoid unnecessary peaks of power consumption. For this reason, the number of AAPs simultaneously recharging during this phase was arbitrarily set equal to the number of active AAPs. When this 'constant consumption' phase begins, the solar panels are still producing enough power to recharge the battery. This example, representing a day when the irradiation is particularly low, shows how power constraint (27b) is always satisfied.

[3]https://www.futurasun.com/wp-content/uploads/2020/10/2020_FuturaSun_60p_260-285W_en.pdf?x78774

[4]http://www.farnell.com/datasheets/3170915.pdf

The optimization of the CS design is repeated using different values of the following variables:

- *mission duration*, which measures the amount of time during which the network is continuously operated;
- *starting time*, which indicates at what time the network starts operating (this is assumed to be the same every day);
- *season*, which is a binary variable: 'winter' goes from the 21$^{\text{st}}$ of September to the 21$^{\text{st}}$ of March, while 'summer' covers the remaining time.

These variables influence the CS design in different ways: the first modifies the power profile shape shown in Fig. 4, whereas starting time and season affect the irradiation data $I_{\text{rr}}(t)$. This sensitivity analysis is summarized in Figs. 9a and 9b, which show how the cost of the system is affected by the three aforementioned variables, respectively for the winter and summer scenarios. The dotted line is included for comparison with the grid-connected case in a urban scenario, which is explained in more depth in Fig. 11. In both seasons, the effect of the mission duration is particularly marked if the mission starts in the afternoon. This is because, when the solar irradiation is low, the task of satisfying the load is left to the battery pack alone, which, as a result, must be made larger. More in general, the greater the mismatch between energy generation and load profile, the larger the battery will need to be. The minimum point of the curves shifts to an earlier starting time as the mission duration grows, suggesting that the cost minimization can only be achieved as a combination of these two variables. While short missions are feasible at almost any time of the day even in winter, longer missions at later times make the system cost soar at a growing pace, due to the decreasing marginal returns of designing a larger ground battery. Apart from this aspect, the curves look similar

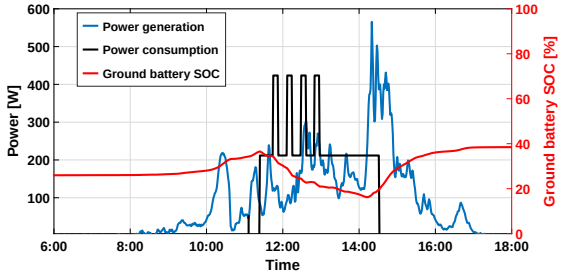

Figure 8: Power profiles and ground battery SOC for a 2 hours mission starting at 11:15 in February.

in winter and summer, with a downward shift in the latter case. However, more pronounced differences can be expected if the 'summer' season is restricted to the actual summer, instead of half a year. Fig. 10 shows how the cost of the

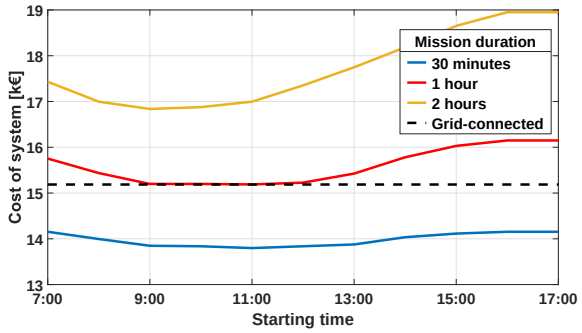

(a) Winter

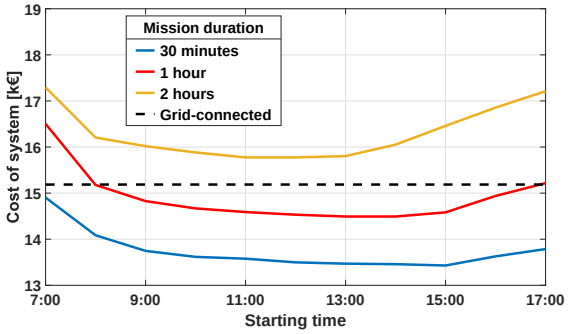

(b) Summer

Figure 9: Cost of the whole system, with 20 users and $Q = 200$ Mb, compared to grid-connected urban scenario.

system and the energy spent per data harvesting cycle change according with the number of ground users and the amount of data to be received from each of these. Both variables have similar effects: the energy spent by an AAP to complete a data harvesting cycle grows at a quasi-constant pace, whereas the charging station cost grows intermittently, together with the number of active AAPs. The latter represents the main voice of expense for the system.

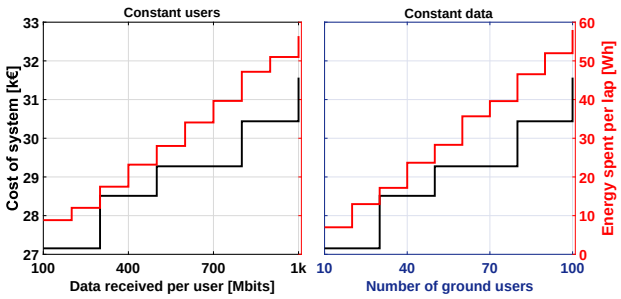

Figure 10: Cost of charging station and energy consumption trends as a function of variable data size and number of users.

A cost comparison is presented in Fig. 11 between the off-grid system described in this work and a grid-connected scenario with the same modes of operation (UAV-based, mission of 2 hours, starting at 11:15). The left hand side of the histogram shows the cost breakdown of the energy-neutral CS, while the right hand side shows the voices of expense for the grid-connected scenario, namely the cost of connecting to the electricity grid and that of the consumed energy. The cost of the UAVs is the same on both sides, so the y-axis is cut to improve readability. The cost of energy was calculated as a cumulative sum on 10 years, assuming a fixed cost of 0.17€/kWh (average cost of electricity in the UK). The cost of connecting the system to the electricity grid was estimated using an online tool provided by an electricity provider in the UK[5], assuming a distance from the substation of 10 meters both in the rural and the urban scenarios. It can be deduced that the installation of a PV-based off-grid charging station is particularly advantageous in rural areas, while the two options have comparable costs in urban areas. It can be observed in Fig. 9 how short missions taking place during the day make the off-grid option less expensive than a grid-connected urban scenario. For longer missions, or when these start later in the day, the EN charging station is only advantageous when compared to the rural scenario, which would be feasible for continuous or nearly-continuous service.

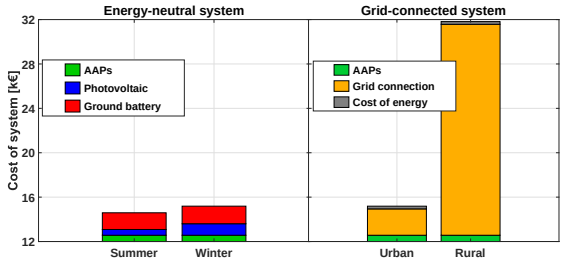

Figure 11: Cost comparison between EN system designed for summer or winter and a grid-connected one in urban or rural area.

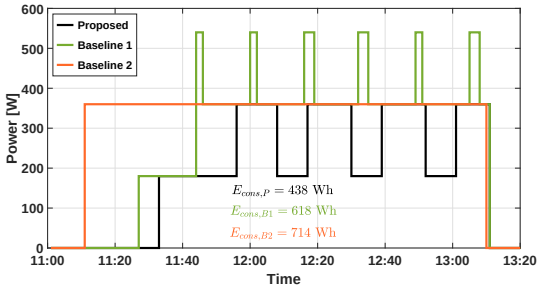

Figure 12: Load profiles comparison between the proposed method and the two baselines.

A cost comparison is carried out between the proposed method and two baseline scenarios considering the same target area, UAV type, and mission duration:

- Baseline 1: The load profile is formed by considering UAVs hovering all the time [12];
- Baseline 2: The CS is designed considering a constant power consumption, corresponding to 2 tethered UAVs [11].

The resulting load profiles can be observed in Fig. 12: the green and orange curves represent the load profiles from Baselines 1 and 2, respectively. In Baseline 1, the UAVs are hovering all the time, thereby reducing their active time, with

[5]https://www.northernpowergrid.com/quick-calculator

Table III: Numerical comparison between proposed methodology and two baseline scenarios.

	N_{aap}	N_{pv}	Battery capacity [Wh]	Total cost [£]
Proposed	3	2	936	13,814.85
Baseline 1	4	3	1273	18,489.46
Baseline 2	3	3	1498	14,538.50

higher peaks of power consumption and the need for an extra UAV; As reported in the figure, the proposed solution has the lowest value of energy consumption by a margin of over 50%, which could be even higher for longer missions. Furthermore, as reported in Table III, the higher load profiles clearly affect the initial cost, either due to the larger CS or to the larger fleet of UAVs. However, the effect of the latter is prominent due to the high cost of UAVs. This explains why, despite consuming less energy than Baseline 2, Baseline 1 is by far the most expensive option.

V. Conclusion and future work

In this article, a holistic design methodology was proposed for a cost-efficient UAV-based EN system for the data harvesting of IoT nodes. This methodology minimizes the investment cost by acting on the planning (how), scheduling (when), and energy supply of the AAP mission.

The main engineering insights derived from the results of this study are listed below:

- The clustering protocol adopted in this study reduces the time and energy an AAP needs to complete a cycle of data harvesting, compared to other benchmark protocols. This gap gets wider for higher numbers of users, up to a 50% energy and time saving in our simulation setups. The same is true for the cost of the system, which has a linear relation with the data exchange.
- For short missions (30 minutes) the investment cost of the system is minimized when the mission starts in the late morning in winter, or in the early afternoon in summer. Earlier times are preferred with longer missions. These cost variations between seasons are mainly due to the PV size required, while mission duration and time mostly affect the ground battery size. However, the larger portion of the investment cost is represented by the AAPs.
- In an urban setting, an EN UAV-based system has an investment cost comparable to that of a grid-connected one, whereas it is much cheaper in rural areas, even for long missions.

The optimal solution is highly dependant on the aforementioned time variables, and the EN option becomes anti-economical when long missions are planned, especially in winter or at night. These issues could be tackled by diversifying the energy sources, which would complicate both the system design and operation, thus representing an interesting topic for future work.

Acknowledgment

This work is supported by the project PAINLESS which has received funding from the European Union's Horizon 2020 research and innovation programme under grant agreement No 812991.

References

[1] Fotouhi, Azade, et al. "Survey on UAV Cellular Communications: Practical Aspects, Standardization Advancements, Regulation, and Security Challenges," *IEEE Commun. Surv. and Tut. 21.4 (2019)*: 3417-3442.

[2] 3GPP; Technical Specification Group Services and System Aspects; "Unmanned Aerial System (UAS) support in 3GPP"; Stage 1; Release 17.

[3] Javidsharifi, Mahshid, et al. "Optimum Sizing of Photovoltaic and Energy Storage Systems for Powering Green Base Stations in Cellular Networks." *Energies 14.7 (2021):* 1895.

[4] Marsan, Marco Ajmone, et al. "Towards zero grid electricity networking: Powering BSs with renewable energy sources," in *IEEE international conf. on commun. workshops (ICC),* IEEE, 2013.

[5] Song J, Krishnamurthy V, Kwasinski A, Sharma R, "Development of a Markov-chain-based energy storage model for power supply availability assessment of photovoltaic generation plants", in *IEEE Trans. on Sustain. Energy. 2012 Sep 10;4(2):*491-500.

[6] Chamola V, Sikdar B, "Outage Estimation for Solar Powered Cellular Base Stations", in *Proceedings of the 2015 IEEE Int. Conf. on Commun. (ICC),* London, UK, 8–12 June 2015; pp. 172–177.

[7] Ibrahim Anwar, et al. "A novel sizing method of a standalone photovoltaic system for powering a mobile network base station using a multi-objective wind driven optimization algorithm," in *Energy Conversion and Management 238 (2021):* 114179.

[8] M. Virgili, A. J. Forysth and P. James, "A Multi-Objective Genetic Algorithm Methodology for the Design of Standalone Energy Systems," in *2021 IEEE Design Methodologies Conf. (DMC),* 2021, pp. 1-6.

[9] Chiaraviglio, Luca, et al. "Minimum cost design of cellular networks in rural areas with UAVs, optical rings, solar panels, and batteries," in *IEEE Trans. on Green Commun. and Netw. 3.4 (2019):* 901-918.

[10] Chiaraviglio, Luca, et al. "Optimal design of 5G networks in rural zones with UAVs, optical rings, solar panels and batteries",in *Proceedings of the 20th International Conf. on Transparent Optical Networks (ICTON), Bucharest, Romania, 1–5 July 2018;* pp. 1–4.

[11] Amorosi, L.; Chiaraviglio, L.; Galan-Jimenez, J. "Optimal energy management of UAV-based cellular networks powered by solar panels and batteries: Formulation and solutions," in *IEEE Access 2019, 7:* 53698–53717.

[12] Galán-Jiménez J, Moguel E, García-Alonso, J, Berrocal J, "Energy-efficient and solar powered mission planning of UAV swarms to reduce the coverage gap in rural areas: The 3D case," in *Ad Hoc Netw. 2021, 118, 102517.*

[13] Javidsharifi, Mahshid, et al. "Optimum sizing of photovoltaic-battery power supply for drone-based cellular networks." in *Drones 5.4 (2021):* 138.

[14] A. Al-Hourani, S. Kandeepan, and S. Lardner, "Optimal LAP altitude for maximum coverage," in *IEEE Wireless Commun. Lett.*, vol. 3, no. 6, pp. 569–572, Dec. 2014.

[15] M. Alzenad, A. El-Keyi, F. Lagum, and H. Yanikomeroglu, "3-D placement of an unmanned aerial vehicle base station (UAV-BS) for energy-efficient maximal coverage," in *IEEE Wireless Commun. Lett.*, vol. 6, no. 4, pp. 434–437, Aug. 2017.

[16] M. Mozaffari, W. Saad, M. Bennis, and M. Debbah, "Efficient deployment of multiple unmanned aerial vehicles for optimal wireless coverage," in *IEEE Commun. Lett.,* vol. 20, no. 8, pp. 1647–1650, Aug. 2016. 69.5 (2021): 3352-3366.

[17] N. Babu, C. B. Papadias and P. Popovski, "Energy-Efficient 3D Deployment of Aerial Access Points in a UAV Communication System," in *IEEE Commun. Lett.*, vol. 24, no. 12, pp. 2883-2887, Dec. 2020.

[18] J. Sun and C. Masouros, "Deployment strategies of multiple aerial BSs for user coverage and power Efficiency Maximization," in *IEEE Trans. Commun.,* vol. 67, no. 4, pp. 2981–2994, Apr. 2019.

[19] Valiulahi, Iman, and Christos Masouros. "Multi-UAV Deployment for Throughput Maximization in the Presence of Co-Channel Interference." in *IEEE Internet of Things Journal* 8.5 (2020): 3605-3618.

[20] Zhou X, Yan S, Shu F, Chen R, Li J, "UAV-Enabled Covert Wireless Data Collection", in *IEEE Journal on Selected Areas in Commun. 2021 Jun 14;39(11):*3348-62.

[21] Yan S, Hanly SV, Collings IB, "Optimal Transmit Power and Flying Location for UAV Covert Wireless Communications", in *IEEE Journal on Selected Areas in Commun. 2021 Jun 16;39(11):*3321-33.

[22] N. Zhao et al., "Joint Trajectory and Precoding Optimization for UAV-Assisted NOMA Networks," in *IEEE Trans. on Commun.,* vol. 67, no. 5, pp. 3723-3735, May 2019.

[23] Zeng Y, Xu J, Zhang R. "Energy Minimization for Wireless Communication with Rotary-Wing UAV", *IEEE Transactions on Wireless Commun.*, 2019 Mar 8;18(4):2329-45.
[24] Jing, Xiaoye, Jingcong Sun, and Christos Masouros, "Energy Aware Trajectory Optimization for Aerial Base Stations." in *IEEE Trans. on Commun.*
[25] N. Babu, M. Virgili, C. B. Papadias, P. Popovski and A. J. Forsyth, "Cost- and Energy-Efficient Aerial Communication Networks With Interleaved Hovering and Flying," in *IEEE Trans. on Vehicular Technology,* vol. 70, no. 9, pp. 9077-9087, Sept. 2021.
[26] Mazaherifar A, Mostafavi S, "UAV Placement and Trajectory Design Optimization: A Survey," in *Wireless Personal Commun. 2021 Dec* 1:1-20.
[27] J. Holis and P. Pechac, "Elevation Dependent Shadowing Model for Mobile Communications via High Altitude Platforms in Built-Up Areas," in *IEEE Trans. on Antennas and Propagation, vol. 56, no. 4, pp. 1078-1084, April 2008.*
[28] P. Yang, X. Xi, T. Q. S. Quek, J. Chen and X. Cao, "Power Control for a URLLC-Enabled UAV System Incorporated With DNN-Based Channel Estimation," in *IEEE Wireless Commun. Lett., vol. 10, no. 5, pp. 1018-1022, May 2021.*
[29] Rokrok E, Javidsharifi M, Pourroshanfekr H, Javidsharifi B, "Adaptive Nonlinear Control Scheme for Three-Phase Grid-Connected PV Central Inverters" in *Proceedings of 29th Int. Power System Conf. (PSC), Terhan, Iran,* 27 October 2014; pp. 1-7.
[30] "Travelling Salesman Problem", availabe online at https://www.mathworks.com/matlabcentral/fileexchange/46629-tsp-zip.
[31] Sonia Leva, Alfredo Nespoli, Silvia Pretto, Marco Mussetta, Emanuele Ogliari, September 23, 2020, "Photovoltaic power and weather parameters", in *IEEE Dataport, doi: https://dx.doi.org/10.21227/42v0-jz14.*
[32] Javidsharifi, Mahshid, et al, "Effect of Battery Degradation on the Probabilistic Optimal Operation of Renewable-Based Microgrids" in *Electricity 2022, 3, 53-74.*
[33] Berliner, H. J. "An Examination of Brute Force Intelligence." *In IJCAI* (pp. 581-587), 1981, August.
[34] A. Goldsmith, Wireless communications. Cambridge university press, 2005.

Marco Virgili (Student Member, IEEE) is an early stage researcher at Lyra Electronics Limited for the EU H2020 ITN project PAINLESS, and he is enrolled as a PhD student at The University of Manchester, UK. He received both his BSc and a MSc degree in Energy Engineering from Sapienza University of Rome, Italy, in 2015 and 2019, respectively. During his PhD, he was a visiting student at the University College of London, UK, and at Aalborg University, Denmark. His research interests include power electronics, automated design methodologies, renewable energy, and machine learning. He is currently working on design automation techniques for distributed energy systems.

Nithin Babu (Student Member, IEEE) is an early stage researcher at Alba, The American college of Greece for the EU H2020 ITN project PAINLESS and he is enrolled as a Ph.D student at Aalborg University, Denmark. He received the B.Tech degree in Electronics and Communication Engineering from CUSAT, India, in 2013, and the M.Tech degree in Communication Systems Engineering from Indian Institute of Technology, Patna, India in 2016. During his M.Tech, he was a DAAD exchange student at Vodafone chair, TU Dresden and was awarded as the best student in order of merit. His research interests include UAV communication, LoS- MIMO systems, mm-wave communication.

Mahshid Javidsharifi (Student Member, IEEE) received her MSc in Electrical Engineering from Lorestan University, Iran in 2015 with highest honors. Her master thesis was devoted to photovoltaic systems. She was awarded as the Recognized Researcher of Lorestan University, in 2014 and 2015. She has published ten journal and several conference papers. She was a visiting researcher at the Department of Energy Technology, Aalborg University from September 2018 to April 2019. Her research interests include energy management of renewable-based microgrids, photovoltaic systems, PV systems modelling, integration of renewable energy sources and storage devices. In July 2019, she joined Aalborg University (AAU) in Aalborg, Denmark, as an early-stage researcher (ESR #3) for the European ITN Project PAINLESS (funded by the European Union's Horizon 2020 research and innovation programme under the Marie Sklodowska-Curie grant agreement No 812991), for which she works on the topic of photovoltaic energy supply for future energy neutral base stations.

Iman Valiulahi (Student Member, IEEE) Iman Valiulahi received the B.Sc. degree in electrical engineering with majors in electronics from the University of Isfahan, Isfahan, Iran, in 2015, and the M.Sc. degree (first place) in telecommunication engineering from Iran University of Science and Technology, Tehran, Iran, in 2018. During his master project, he was engaged in a variety of signal processing problems, such as super-resolution, one-bit compressed sensing, OFDM radar, and blind deconvolution. In 2019, he joined University College London, London, U.K., as an early stage researcher for the European ITN Project PAINLESS, for which he will work on the topic of energy balancing and optimization framework for future energy-neutral HetNets access points.

Christos Masouros (Senior Member, IEEE) is since 2019 a Full Professor of Signal Processing and Wireless Communications in the Information and Communication Engineering research group, Dept. Electrical and Electronic Engineering, and affiliated with the Institute for Communications and Connected Systems, University College London. His research interests lie in the field of wireless communications and signal processing with particular focus on Green Communications, Large Scale Antenna Systems, Integrated Sensing and Communications. He was the co-recipient of the 2021 IEEE SPS Young Author Best Paper Award. He was the recipient of the Best Paper Awards in the IEEE GlobeCom 2015 and IEEE WCNC 2019 conferences, and has been recognised as an Exemplary Editor for the IEEE Communications Letters, and as an Exemplary Reviewer for the IEEE Transactions on Communications. He is an Editor for IEEE Transactions on Wireless Communications, the IEEE Open Journal of Signal Processing, and Editor-at-Large for IEEE Open Journal of the Communications Society. He has been a Guest Editor for a number of IEEE Journal on Selected Topics in Signal Processing and IEEE Journal on Selected Areas in Communications issues. He is a founding member and Vice-Chair of the IEEE Emerging Technology Initiative on Integrated Sensing and Communications, and Chair of the IEEE Green Communications Computing Technical Committee, Special Interest Group on Green ISAC.

Andrew J. Forsyth (Senior Member, IEEE) received the B.Sc.(Eng.) degree in electrical engineering from Imperial College, London, U.K., in 1981, and the Ph.D. degree in power electronics from the University of Cambridge, Cambridge, U.K., in 1987. He was a Design Engineer with GEC Electrical Projects, Ltd., from 1981 to 1983, a Lecturer with the University of Bath from 1986 to 1990, and a Lecturer/Senior Lecturer with Birmingham University from 1991 to 2004. Since 2004, he has been a Professor of power electronics with the University of Manchester, Manchester, U.K. His research interests include high-frequency converters and magnetic components, converter modeling and control, and aerospace and electric vehicle applications.

Tamas Kerekes (Senior Member, IEEE) has obtained the Electrical Engineer diploma in 2002 from Technical University of Cluj, Romania, with specialization in Electric Drives and Robots. In 2005, he graduated the Master of Science program at Aalborg University, Department of Energy Technology in the field of Power Electronics and Drives. In 2009 he has obtained the PhD degree from the Department of Energy Technology, Aalborg University. The topic of the PhD program is: "Analysis and modeling of transformerless PV inverter systems". He is currently employed at Aalborg University as an Associate professor and is doing research within the field of grid connected renewable energy systems focusing on different grid forming and grid following control algorithms for power electronic converters for renewable energy systems with storage solutions.

Constantinos B. Papadias (Fellow, IEEE) is the Executive Director in the Research, Technology, and Innovation Network (RTIN) of the American College of Greece. He is also Adjunct Professor at Aalborg University and at the University of Cyprus. He received the Diploma of Electrical Engineering from the National Technical University of Athens (NTUA) in 1991 and the Doctorate degree in Signal Processing (highest honors) from the ENST, Paris, France, in 1995. He has published over 230 papers and 3 books and has received over 10000 citations for his work, with an h-index of 46. His main research interests include signal processing for wireless communications, MIMO systems, antenna arrays, and spectrum sharing.